

PROCEEDINGS OF SPIE

[SPIDigitalLibrary.org/conference-proceedings-of-spie](https://spiedigitallibrary.org/conference-proceedings-of-spie)

Monte-Carlo based simulations of photothermal response of nerve tissue for laser wavelengths of 1455 nm, 1490 nm, 1550 nm

Türker Burhan, Merve, Tozburun, Serhat

Merve Türker Burhan, Serhat Tozburun, "Monte-Carlo based simulations of photothermal response of nerve tissue for laser wavelengths of 1455 nm, 1490 nm, 1550 nm," Proc. SPIE 11238, Optical Interactions with Tissue and Cells XXXI, 1123814 (20 February 2020); doi: 10.1117/12.2543868

SPIE.

Event: SPIE BiOS, 2020, San Francisco, California, United States

Monte-Carlo based simulations of photothermal response of nerve tissue for laser wavelengths of 1455 nm, 1490 nm, 1550 nm

Merve Turker Burhan^{a,b} and Serhat Tozburun^{*a,b,c}

^aIzmir Biomedicine and Genome Center, Mithatpasa St. 58/5 Balcova, TURKEY 35330; ^bIzmir International Biomedicine and Genome Institute, Dokuz Eylul University, Mithatpasa St. 58/5 Balcova, TURKEY 35330; ^cDepartment of Biophysics, Faculty of Medicine, Dokuz Eylul University, Mithatpasa St. 58/5 Balcova, TURKEY 35330

ABSTRACT

Electrical nerve stimulation (ENS) technique has been tested on nerve mapping devices, which are intraoperative diagnostic tools. However, these technologies suffer from general limitations. Optical Nerve Stimulation (ONS) has been a developing technique as a potential alternative to ENS. This new technique using infrared laser radiation can offer many advantages, including a non-contact stimulation mode, improved spatial selectivity, and elimination of stimulation artifacts. However, the stimulation parameters, including laser power, beam diameter, and surface scanning speed, provide a large variable matrix that must be optimized for consistent and reliable nerve mapping using ONS. This preliminary study explores a computational tool to provide a guiding map for determining optimal stimulation parameters for laser-scanning subsurface ONS. It consisted of three parts: (1) Monte Carlo simulations for generating laser energy distribution in the tissue sample, (2) laser-scanning model by moving the heat source at the surface, and (3) thermal transfer simulations to calculate the tissue temperature. The tool was tested on laser wavelengths of 1455 nm, 1490 nm, and 1550 nm. According to the results of calculations, nerve temperature maps were generated for those wavelengths. Each map demonstrated specific optimal parameter values to reach the nerve activation temperature. Additionally, the results of laser power densities at the lowest scanning speeds of 0.4 mm/s in x-axis and 0.5 mm/s in y-axis showed proximate results with our previous study about ONS on rat model. With further development, this tool may hold promise in the development of an intraoperative optical stimulus device for surgical applications.

Keywords: Computer simulations, Monte Carlo, optical properties, optical nerve stimulation, cavernous nerves

1. INTRODUCTION

Optical nerve stimulation has been a developing technique as a potential alternative to electrical nerve stimulation (ENS). ENS technique has been tested on intraoperative nerve mapping devices [1]. However, these technologies suffer from the general limitations caused by ENS, including the need for physical contact between the electrode and nerve, lack of spatial selectivity, and electrical stimulation artifacts. In contrast, ONS can offer many advantages over ENS limitations for both scientific studies and clinical applications [2]. Recently, we have demonstrated subsurface ONS in the rat model as an intermediate step towards a support device for intraoperative diagnosis and preservation of the cavernous nerve tissue [3]. However, the stimulation parameters indicated a large matrix of variables that need to be optimized to perform a safe and efficient ONS. Stimulation variables might include laser power, beam diameter, and surface scanning speed.

The ONS technique mainly relies on the interaction of infrared light with the soft tissue. This interaction is described as a thermal process, which is the result of light emission in biological tissue. Monte Carlo simulation [4] based on statistically random physical quantity sampling has become the gold standard for analyzing light scattering in biological tissue. The applicability of this technique to multilayered tissue provides a platform to quantitatively examine the photothermal response of biological tissues [5]. Therefore, ONS can be studied in the framework of a photothermal process to obtain preliminary results for pre-clinical applications.

*serhat.tozburun@ibg.edu.tr; phone 90 232 299-5101; fax 90 232 277-6353 tozburunlab.com

This study aims to further investigate the previously reported Monte-Carlo based photothermal simulation model of the cavernous nerve that lies beneath a fascia layer along the prostate surface [6]. The advanced model intends to generate a map of nerve temperature as a function of laser power density and surface scanning speed for different laser wavelengths (1455 nm, 1490nm, 1550 nm).

2. METHODOLOGY

The calculation tool consisted of three parts. The first part was Monte Carlo modeling of laser radiation in tissue. The multi-layer approach provided by the Monte Carlo technique was utilized to model the three-dimensional probability distribution of the absorption and scattering events of laser energy. The absorption and scattering coefficients defined these events at each step of light propagation in the tissue sample. The step size was randomly sampled according to the optical properties (the absorption coefficient and scattering coefficient). Additional optical properties (i.e., refractive index and anisotropy factor) were used in the calculations to determine the propagation direction of light in the tissue sample. A three-layered medium consisting of fascia, nerve, and prostate from top to bottom defined the tissue model. The physical dimensions of the tissue model were 4 mm (x, y) x 3 mm (z), where z is the depth of tissue. This three-dimensional tissue structure was determined to be a single mesh size of 40 μm x 40 μm x 40 μm with a 100 x 100 x 75 mesh system. The nerve layer was placed along the y-axis. Each layer of the three-dimensional tissue model was exemplified with the thickness and laser wavelength-dependent optical properties. The source codes were available in Ref. [5, 7]. The calculated energy absorption profile was convoluted to obtain a pooled Gaussian laser beam of 0.5 mm in diameter.

The second part was the laser-scanning model over the tissue surface. To model the laser surface scanning, the distribution of the laser energy used as a heat source was moved at a constant speed on the x-axis and the y-axis, respectively, as shown in Figure 1.

Figure 1 shows a representative model of tissue sample consisting of fascia (yellow), nerve (white), and prostate (brown) layers. The fascia layer covered both the nerve and the prostate layers. A 300 μm diameter nerve was placed between the prostate and fascia layers along the y-axis and centered on both axes. The laser beam (red) began scanning on the x-axis and then on the y-axis.

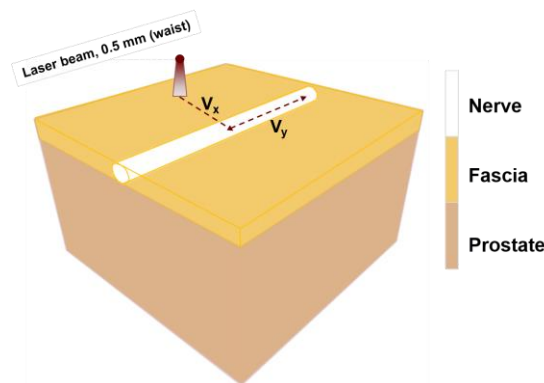


Figure 1. A 3D (x-axis, y-axis and depth) representation of the tissue model that contains the fascia (yellow), nerve (white) and prostate (brown) layers. The diameter of the nerve is 300 μm and the nerve extends along the y-axis under fascia. Surface scanning starts in x-axis and goes toward the nerve and after reaching the nerve, it continues in y-axis.

The last part was thermal transfer simulations to calculate tissue temperature. We used a time-dependent finite difference element method to simulate heat transfer in three-dimensional tissue according to the described laser surface scanning model. Time-dependent laser-induced heat transfer calculations were based on Pennes' bio-heat transfer equation as follows:

$$\rho C \frac{\partial T}{\partial t} = k \nabla^2 T + Q$$

ρ is the density, C is the specific heat, and k is the thermal conductivity. These parameters were considered as constant thermal properties of the anisotropic medium. T is the resulting tissue temperature obtained in functions of time and space. Q represents the heat source of the laser irradiation (computed by Monte Carlo simulation). The initial tissue temperature was set to 37°C. The time step to advance the temperature solutions of the surface scan was 11 μ s. To accurately model the distribution of absorbed radiation in tissue layers, the required unit-weighted photons were used as one million, depending on the spatial resolution in the simulation. At each time step, the heat source was moved according to the defined speed in the x-axis or y-axis. The calculated tissue temperature profiles represented the effects of the laser-scanning model.

Besides, laser-induced thermal damage was estimated in a model based on the Arrhenius integral using calculated tissue temperature profiles ($T(t)$) as follows [8]:

$$\Omega(t) = \xi \int_0^{\tau} e^{\frac{E_a}{RT(t)}} dt$$

Ω is the degree of tissue damage, ξ is the frequency factor, τ is the total heating time, E_a is the activation energy of the transformation, R is the universal gas constant, and T is the absolute temperature of the tissue in degrees Kelvin. When Ω reaches to 1, the degree of tissue damage is associated with thermal necrosis.

Considering the results of our previous study [3], 1455 nm, 1490 nm, and 1550 nm were selected as laser wavelengths in computer simulation studies. Table 1 summaries the thermal properties, thermal kinetic properties, layer thicknesses, and optical properties of the model tissue at 1455 nm, 1490 nm, and 1550 nm. The thickness of the fascia layer above the nerve was assumed according to the ONS of the rat cavernous nerve [3].

Table 1. Optical Properties at 1455 nm, 1490 nm, 1550 nm, layer thicknesses, and thermal properties.

Optical Properties and Layer Thicknesses			
	Fascia	Nerve (white matter)	Prostate
1455 nm			
Absorption coefficient, cm^{-1}	9 [9]	42 [10]	56.81 [11, 12]
Reduced scattering coefficient, cm^{-1}	18 [9]	5.93 [11]	5.82 [11]
Anisotropy factor	0.76 [9]	0.9 [13]	0.9 [13]
Refractive index	1.319 [14]	1.467 [15]	1.4 [15]
Layer thickness, cm	0.011[3]	0.03 [16]	0.259
1490 nm			
Absorption coefficient, cm^{-1}	7 [9]	28 [10]	53.9 [11, 12]
Reduced scattering coefficient, cm^{-1}	15 [9]	5.9 [11]	5.61 [11]
Anisotropy factor	0.8 [9]	0.9 [13]	0.9 [13]
Refractive index	1.318 [14]	1.467 [15]	1.4 [15]
Layer thickness, cm	0.038 [3]	0.03 [16]	0.232
1550 nm			
Absorption coefficient, cm^{-1}	4 [9]	20 [10]	32.16 [11, 12]
Reduced scattering coefficient, cm^{-1}	12 [9]	5.86 [11]	5.28 [11]
Anisotropy factor	0.87 [9]	0.9 [13]	0.9 [13]
Refractive index	1.317 [14]	1.467 [15]	1.4 [15]
Layer thickness, cm	0.045 [3]	0.03 [16]	0.225
Thermal Properties			
Thermal conductivity, $\text{W/m}^{\circ}\text{C}$	0.47 [17]	0.503 [18]	0.5 [19]
Specific heat, $\text{J/kg}^{\circ}\text{C}$	3.2 [17]	3.6 [18]	3.78 [19]
Density, kg/m^3	1.085e ⁶ [17]	1.027e ⁶ [18]	1.06e ⁶ [19]
Thermal Kinetic Properties			
	Retina Cell		
Frequency factor, s^{-1}	1.6e ⁵⁵ [20]		
Activation energy, J/mol	3.4e ⁵ [20]		
Universal gas constant, J/K mol	8.32		

3. RESULTS

Figure 2 shows the transient tissue temperature distribution solved by a time-dependent laser-induced heat transfer equation. These en-face frames represented changes in the temperature profiles of a subsurface slice of the tissue sample. This subsurface slice was 0.52 mm deep from the surface. In this simulation, the laser power was 100 mW at the wavelength of 1550 nm (the corresponding laser power density was 51 W/cm² for a beam diameter of 0.5 mm). The scanning speed was set to 1.2 mm/s on the x-axis and 0.5 mm/s on the y-axis. Total scanning time was calculated as 4 s (from Panel a to Panel d in Figure 2). The maximum tissue temperature reached during the surface scanning was 63.4°C.

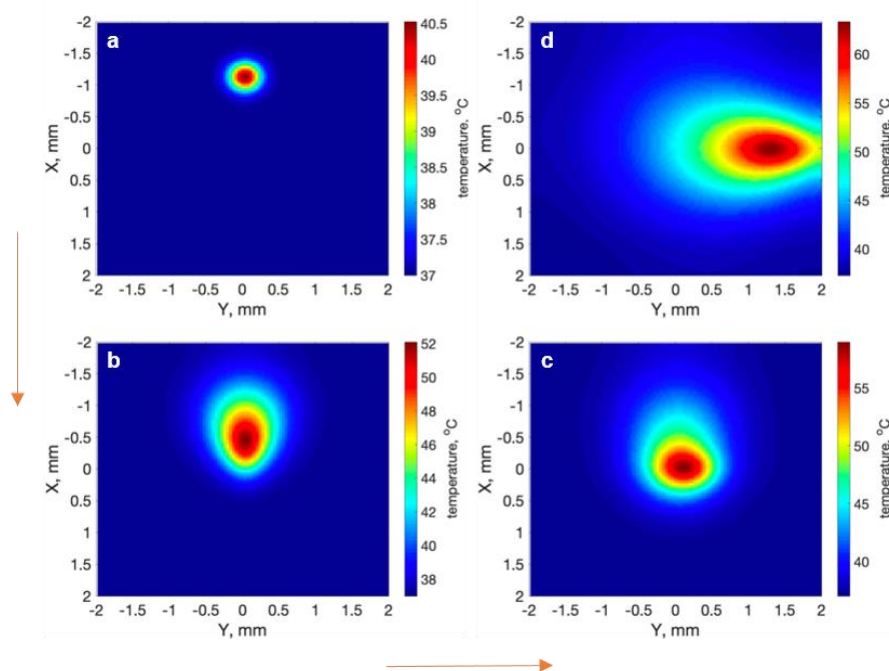


Figure 2. En face frames of transient tissue temperature profiles (from upper left to upper right). Orange arrows show the transition of temperature profile in time, in sequence. (a) Starting of laser surface scanning on x-axis. (b) Surface scanning forward through the x-axis. (c) Facing with nerve at the center of tissue. (d) Surface scanning on nerve through the y-axis.

To map the maximum nerve temperature, the simulation procedure was repeated for laser power density ranging from 2.55 W/cm² to 51.0 W/cm² and different scanning speeds that changed from 0.4 mm/s to 1.2 mm/s for the x-axis, and from 0.5 mm/s to 2.0 mm/s for the y-axis. With this approach, three guiding maps were created for the laser wavelengths of 1455 nm (Figure 3), 1490 nm (Figure 4) and 1550 nm (Figure 5). Wavelength dependent optical properties changed the absorbed photon weight distribution ultimately affecting temperature profile. Thermal damage was calculated by using Arrhenius integral for each laser power density. The solid white lines on the maps show the thermal damage threshold with the calculated critical temperature of 48.4 °C. The thermal damage threshold shifted on the power density axis with changing laser wavelengths.

The reported critical nerve temperature for successful optical nerve stimulation in the rat model was ~43°C [21]. The optimal power density to reach the nerve temperature at >43°C varied as a function of laser wavelengths. At 1455 nm, we estimated the optimal power density as 7.6 W/cm² at the scanning speeds of 1.2 mm/s in the x-axis and 0.7 mm/s in the y-axis. Besides, the estimated laser power density was 12.7 W/cm² at 1490 nm and 15.3 W/cm² at 1550 nm at the scanning speeds of 1.2 mm/s in the x-axis and 1.0 mm/s in the y-axis.

At the lowest scanning speeds of 0.4 mm/s in the x-axis and 0.5 mm/s in the y-axis, the optimal power densities for successfully ONS were estimated as 7 W/cm², 8 W/cm², 10.2 W/cm² for the wavelengths of 1455 nm, 1490 nm and 1550 nm, respectively. The calculated results for the power densities were very close to the experimentally obtained results presented in the previous study [3].

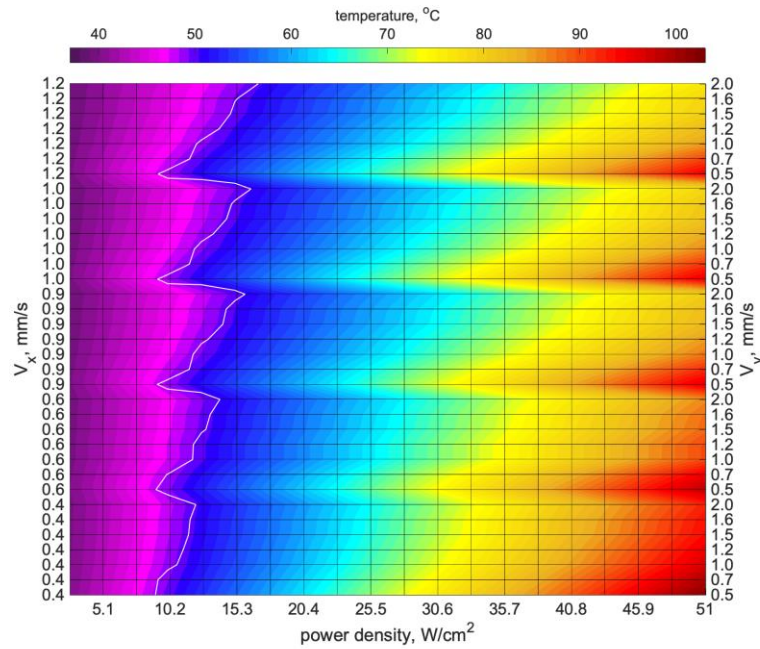


Figure 3. The map of maximum nerve temperature reached during surface scanning as a function of laser power density and surface scanning speed for laser wavelength at 1455 nm. The white solid line indicates the thermal damage threshold caused by the laser radiation at a critical temperature of 48.4°C.

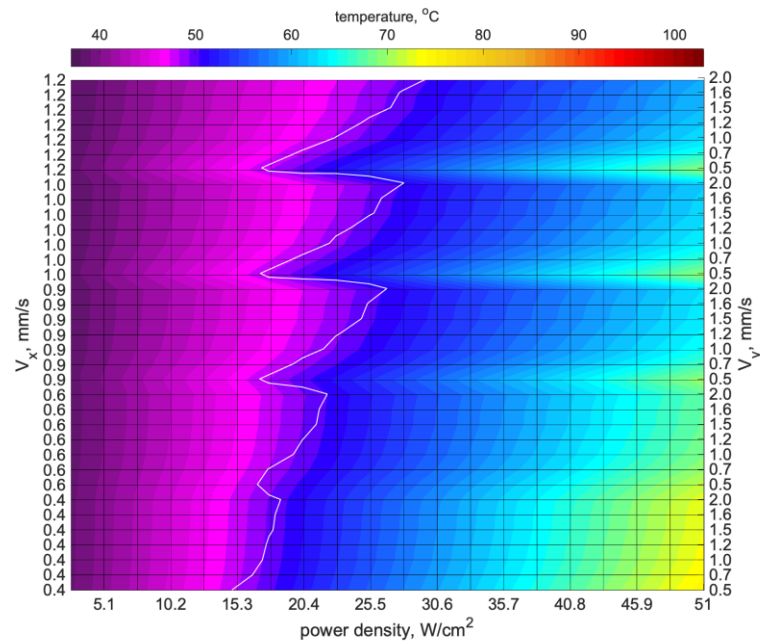


Figure 4. The map of maximum nerve temperature reached during surface scanning as a function of laser power density and surface scanning speed for laser wavelength at 1490 nm. The white solid line indicates the thermal damage threshold caused by the laser radiation at a critical temperature of 48.4°C.

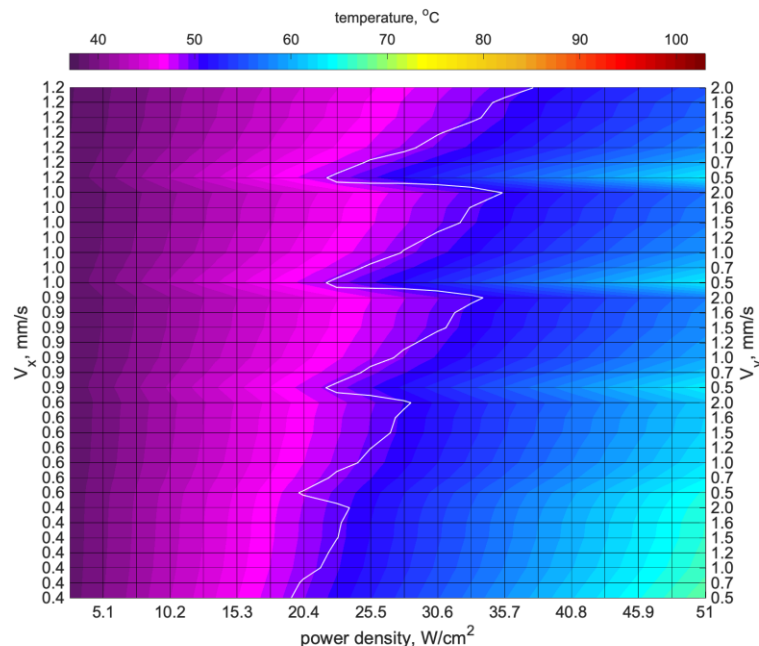


Figure 5. The map of maximum nerve temperature reached during surface scanning as a function of laser power density and surface scanning speed for laser wavelength at 1550 nm. The white solid line indicates the thermal damage threshold caused by the laser radiation at a critical temperature of 48.4°C.

4. DISCUSSION

As an emerging technique, optical nerve stimulation can be used in many complex clinical applications, including nerve mapping. However, the stimulation parameters are highly variable to suggest a reliable, robust and reproducible method. Therefore, critical parameters (i.e., power density, surface scanning speed, and laser wavelength) need to be carefully optimized. This simulation study investigates a calculation tool based on the Monte Carlo algorithm to simulate photothermal modulation of the cavernous nerve underlying a fascia layer along the prostate surface.

There are a few points that should be discussed briefly for future experimental studies and further development of the calculation tool. First, in this study, it is assumed that the absorption and scattering coefficients and thermal properties of the tissue are constant over time. Second, it may also be necessary to investigate the more complex tissue structure involving blood vessels to analyze heat dissipation. Finally, the laser surface scan simulation can be applied to the field at several speeds instead of applying to the lines on both axes to expand the variable matrix of the surface scanning subsurface ONS.

5. CONCLUSIONS

This study successfully demonstrated a computer simulation tool as a complementary component to future pre-clinical and clinical optical nerve stimulation studies. The applicability of the tool for different parameters provides an opportunity to advance improvements. With the numerical specification of the parameters, the necessity for repeated pre-clinical studies will be decreased. With further development, this tool may hold promise for the development of an intraoperative optical stimulus device for surgical applications.

ACKNOWLEDGEMENTS

This work was supported partially by TUBITAK grant No [117E985] and the European Union's Horizon 2020 research and innovation programme under the Marie Skłodowska-Curie grant agreement No [835907]. Serhat Tozburun was supported by the Turkish Academy of Sciences Young Scientists Award Programme (2018 TUBA GEBIP). Merve Turker Burhan was supported by a Turkish Council of Higher Education 100/2000 doctoral scholarship.

REFERENCES

- [1] Takenaka, A., Soga, H., Hinata, N. *et al.*, "Classification of the distribution of cavernous nerve fibers around the prostate by intraoperative electrical stimulation during laparoscopic radical prostatectomy," *International Journal of Impotence Research* 23(2), 56-61 (2011).
- [2] Wells, J., Kao, C., Jansen, E. D. *et al.*, "Application of infrared light for in vivo neural stimulation," *Journal of Biomedical Optics* 10(6), 1-11 (2005).
- [3] Tozburun, S., Lagoda, G. A., Burnett, A. L. *et al.*, "Infrared Laser Nerve Stimulation as a Potential Diagnostic Method for Intra-Operative Identification and Preservation of the Prostate Cavernous Nerves," *IEEE Journal of Selected Topics in Quantum Electronics*, 20(2), 299-306 (2014).
- [4] Wilson, B. C. and Adam, G., "A Monte Carlo model for the absorption and flux distributions of light in tissue," *Medical Physics* 10(6), 824-830 (1983).
- [5] Wang, L. H., Jacques, S. L. and Zheng, Z., "MCML—Monte Carlo modeling of light transport in multi-layered tissues," *Computer Methods and Programs in Biomedicine* 47(2), 131-146 (1995).
- [6] Turker, M. and Tozburun, S., "Simulations for modeling the photothermal response of nerve tissue," *Proceedings of SPIE* 11079, 110791N (2019).
- [7] Jacques, S. L. and Li, T., "Monte Carlo simulations of light transport in 3D heterogenous tissues (mcxyz.c)," Available at <https://omlc.org/software/mc/mcxyz/index.html>, Version June 1, (2017).
- [8] Henriques, F. C. and Moritz, A. R., "Studies of Thermal Injury: I. The Conduction of Heat to and through Skin and the Temperatures Attained Therein. A Theoretical and an Experimental Investigation," *The American Journal of Pathology* 23(4), 531-549 (1947).
- [9] Kozintseva, M. D., Bashkatov, A. N., Kochubey, V. I. *et al.*, "Optical properties of parietal peritoneum in the spectral range 350-2500 nm," *Proceedings of 9031, 90310E* (2014).
- [10] Dirnagl, U., Villringer, A. and Einhaupl, K. M., [Optical Imaging of Brain Function and Metabolism] Springer US, New York, 53 (1993).
- [11] Jacques, S. L., "Optical properties of biological tissues: a review," *Physics in Medicine and Biology* 58(11), R37-R61 (2013).
- [12] Sordillo, A. L., Pu, Y., Pratavieira, S. *et al.*, "Deep optical imaging of tissue using the second and third near-infrared spectral windows," *Journal of Biomedical Optics* 19(5), 056004 (2014).
- [13] Niemz, M. H., [Laser-Tissue Interactions: Fundamentals and Applications, 3rd Enlarged Edition], Springer, Berlin Heidelberg, 23 (2007).
- [14] Hale, G. M. and Querry, M. R., "Optical Constants of Water in the 200-nm to 200- μ m Wavelength Region," *Applied Optics* 12(3), 555-563 (1973).
- [15] Pawley, J., [Handbook of Biological Confocal Microscopy, 3rd Edition], Springer, New York, 377 (2006).
- [16] Takenaka, A., Murakami, G., Matsubara, A. *et al.*, "Variation in course of cavernous nerve with special reference to details of topographic relationships near prostatic apex: histologic study using male cadavers," *Urology* 65, 136-142 (2005).
- [17] Hardy, L. A., Chang, C.-H., Myers, E. M. *et al.*, "Computer simulations of thermal tissue remodeling during transvaginal and transurethral laser treatment of female stress urinary incontinence," *Lasers in Surgery and Medicine* 49(2), 198-205 (2017).
- [18] Collins, C. M., Smith, M. B. and Turner, R., "Model of local temperature changes in brain upon functional activation," *Journal of Applied Physiology* 97(6), 2051-2055 (2004).
- [19] Manuchehrabadi, N. and Zhu, L., "Development of a computational simulation tool to design a protocol for treating prostate tumours using transurethral laser photothermal therapy," *International Journal of Hyperthermia* 30(6), 349-361 (2014).
- [20] Sramek, C., Paulus, Y., Nomoto, H. *et al.*, "Dynamics of retinal photocoagulation and rupture," *Journal of Biomedical Optics* 14(3), 034007 (2009).
- [21] Tozburun, S., Hutchens, T. C., McClain, M. A. *et al.*, "Temperature-Controlled Optical Stimulation of the Rat Prostate Cavernous Nerves," *Journal of Biomedical Optics* 18(6), 067001 (2013).